

## Localized Photon Lasing in a Polaritonic Lattice Landscape

M. Navadeh-Toupchi<sup>✉</sup>, F. Jabeen,<sup>†</sup> D.Y. Oberli<sup>✉</sup>, and M.T. Portella-Oberli

*Institute of Physics, School of Basic Sciences, Ecole Polytechnique Fédérale de Lausanne, 1015 Lausanne, Switzerland*



(Received 17 March 2020; revised 24 June 2020; accepted 20 July 2020; published 19 August 2020)

Periodic photonic structures have attracted much interest due to their versatility for controlling light propagation. The dispersion of photon modes in photonic lattices exhibits an energy band structure analogous to the electronic one in crystals. An important consequence of the photonic band structure is the localization of light in a band gap, which can be engineered by breaking the translational symmetry introducing a defect in the lattice. Here, we demonstrate experimentally the localization of light in a two-dimensional periodic system of polaritons confined in a patterned microcavity. We generate a self-trapping of light by optically inducing a local breaking of the strong-coupling regime of excitons to photons. In the photon lasing regime we show the existence of confined modes that can be controlled by the shape of the generated defect. We demonstrate single on-site localization with lasing mode at the edge of the Brillouin zone similar to a gap soliton. Our results pave the way for useful tools to optically control localization and propagation of light towards the generation of microlasers.

DOI: 10.1103/PhysRevApplied.14.024055

### I. INTRODUCTION

A photonic crystal [1] is a periodically modulated structure; the resultant photonic dispersion is analogous to the electronic band structure in a solid with multiple bands separated by band gaps. The photonic dispersion presents regions of normal and anomalous dispersion in the same way as band curvature defines positive and negative effective masses in crystalline solids. The dynamics in these systems can be governed by the interplay between dispersion or diffraction and nonlinearity [2]. For instance, in lattices of evanescently coupled waveguides, self-localization of light takes place when on-site nonlinearity balances the diffraction arising from linear coupling effects among adjacent waveguides [3,4]. Localized spatial solitons are generated in this way [4–7]. Therefore, by utilizing the photonic band gap and dispersion relation between photon energy and wave-vector light propagation can be controlled and the realization of optical devices can be achieved. Band-edge lasers [8–12] are realized thanks to small group velocity near the edge of the Brillouin zone. The localization of light can also be induced by locally perturbing the periodicity of the lattice generating a defect state [1]. The microcavity formed from a single defect in a two-dimensional photonic crystal has been used to tailor the spontaneous emission as proposed in Ref. [13] and predicted in Ref. [14]. This approach

features small mode volumes and large cavity  $Q$  factors [15,16]. A defect in a two-dimensional photonic crystal provides a resonant microcavity for achieving lasing [17–19].

In a semiconductor microcavity, the strong coupling between excitons and photons gives rise to two new quasiparticles: the lower polariton (LP) and the upper (UP) polariton [20]. These composite exciton-photon quasiparticles constitute an attractive system for studying nonequilibrium dynamics of many-body systems [21]. These optical microcavities are flexible photonic platforms to engineer potential landscapes giving rise to substantial transport properties and appealing physics and applications [22]. For instance, the two-dimensional polaritonic lattices are periodically modulated microcavities in both transverse directions, and translational invariant with respect to the longitudinal direction. They are constituted of coupled arrays of zero-dimensional polaritons arranged in patterned lattices [23]. The dispersion of LP and UP modes corresponds to a band structure separated by the Rabi coupling energy; it is composed of  $S$  and  $P$  bands, which originate from the spatial overlap of  $s$  and  $p$  levels from polaritons confined in all three spatial directions on adjacent mesas. Polariton propagates in the transverse direction according to the energy-band dispersion. The band structure also has a strong influence on the condensation process and results in the localization of polariton condensates. At the edge of the Brillouin zone with negative effective mass, the repulsive polariton interaction with a spatially localized excitonic reservoir causes an energy blueshift of the condensate into the gap and generates a localized

\*morteza.navadehtoupchi@epfl.ch

<sup>†</sup>Present address: Technische Physik University of Würzburg, Am Hubland 97074 Würzburg, Germany.

gap soliton state [24–26]. It has also been shown that the structure of the localized state depends on the spatial position of excitation [27]. In the regime of weak coupling between excitons and photons, photonic resonator crystals using two-dimensional coupled arrays of vertical-cavity surface-emitting lasers (VCSELs) have led to a coherent supermode emission located at the edge of the Brillouin zone [28–30]. Single-mode lasing was also attained by introducing a defect cavity in VCSEL photonic structures [31–34].

An alternative and still unexplored approach to localize light might be to induce a breakdown of the exciton-photon strong coupling within a spatially limited region in order to destroy the photonic crystal symmetry. Inside this region, the photonic modes differ in energy from those of the polariton modes outside of it and, thus, photon propagation to the outside region is inhibited. A self-trapping of light consequent upon the breakdown of the strong-coupling regime is then expected to be observable in a polaritonic lattice. Moreover, the reduction of the losses by propagation can facilitate a phase transition to photon lasing as observed in VCSELs. Due to the interplay between gain and propagation losses, the lasing from localized photon modes can then be favored in a patterned system blending photons and polaritons.

Here, we report on self-trapping of light and localized photon lasing in a two-dimensional triangular lattice of coupled mesas in a semiconductor microcavity. The scheme we use is based on optically inducing a local breaking of the strong-coupling regime of polaritons. We generate, in this way, a defect in the photonic lattice by quenching any photon propagation outside this local region. Under local and nonresonant optical pumping, we show that lasing gain occurs in the localized excitation region. By controlling the position of the optical excitation, we evidence the dependence of the lasing action due to the optically induced lattice defect, which operates as a microcavity that confines the modes of the laser. Ultimately, we observe experimentally that lasing arises at the edge of the Brillouin zone like a gap soliton, which is due to the balance of the nonlinear autofocusing effect and the anomalous diffraction.

## II. SAMPLE AND EXPERIMENT

### A. Sample

The layout of the sample used to carry out this investigation is shown in Fig. 1(a). The sample is grown by molecular-beam epitaxy on a GaAs substrate. It is a

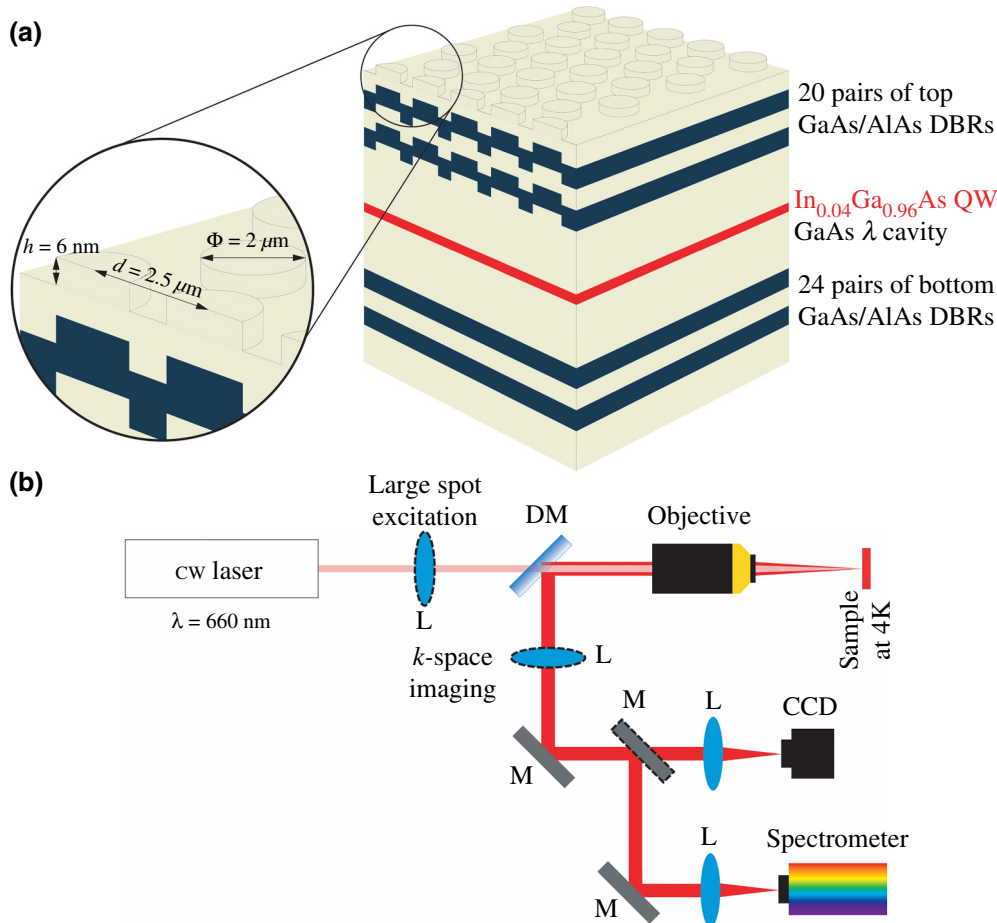


FIG. 1. (a) Schematic drawing of the sample representing the patterned and epitaxial layer structure; DBR stands for distributed Bragg reflector. The inset shows the mesa configuration. (b) Layout of the experimental setup: DM, dichroic mirror; M, mirror; L, lens. Movable parts (lenses and mirror) are drawn with dashed lines.

microcavity made with a GaAs  $\lambda$ -spacer layer and two distributed Bragg reflector (DBR) mirrors consisting of 20 (24) pairs of GaAs/AlAs layers for the top (bottom) mirror. The spacer layer is patterned before the growth of the second DBR of the cavity [35]. The triangular landscape is determined by means of an electron-beam lithography and etching process. The photon traps consist of shallow mesas with a local elevation of 6 nm and a diameter of 2  $\mu\text{m}$  at the surface of the spacer layer. This leads to a local decrease of the microcavity resonance frequency and to a photonic confinement potential of 9 meV. The mesas are equally separated by a distance of 2.5  $\mu\text{m}$  from center to center. The confined photon wave function penetrates into the barrier causing evanescent photonic coupling between neighboring mesas, which induces the formation of a photonic energy band structure. A single  $\text{In}_{0.04}\text{Ga}_{0.96}\text{As}$  quantum well is placed at the antinode of the electromagnetic field in the middle of the spacer layer. The strong coupling between the exciton and photonic modes gives rise to a band structure made of the upper and lower polariton bands corresponding to a Rabi splitting of  $\Omega_R = 3.4$  meV. The exciton energy is  $E_X = 1.4814$  eV. The measured exciton-cavity detuning has a value of 1.5 meV; it is defined as the energy difference between the lowest photonic band and the exciton at the center of the Brillouin zone.

## B. Experimental setup

We excite the sample nonresonantly with a cw laser (Cobolt) operating at 660 nm with a spot size of either 25  $\mu\text{m}$  or 3  $\mu\text{m}$  measured as the full width at half maximum. The layout of the experimental setup is shown in Fig. 1(b). To excite with a small spot size, the laser beam is focused by means of a microscope objective ( $\times 50$ ) with a large numerical aperture (0.42). To obtain a larger spot size, the laser is first sent to an additional lens placed at a distance for which its focal plane coincides with the back Fourier plane of the microscope objective to reduce the laser spot size in the Fourier plane. To avoid thermal heating of the sample, the laser beam is modulated at a 0.6 kHz frequency with a chopper operating with a duty cycle of 6%. The emission of the sample is collected in the reflection configuration with the same objective used for the excitation; it is then focused with a lens of 400-mm focal length on a CCD camera for imaging in real space the emission integrated in energy, which results in a magnification of 100. The spectrally resolved emission is obtained either in the near field or in the far field by imaging the sample surface plane or the Fourier plane of the microscope objective on the entrance slit of the spectrometer that is coupled to a CCD camera. We measure the spatial and the momentum distribution of the emission as a function of energy, which is recorded along the  $x$  direction and the  $\Gamma$ -K direction in the Brillouin zone, respectively. The reciprocal space imaging is used for accessing the

polariton and photonic dispersion curves. The experiments are performed with different excitation pump powers. The sample is placed in a liquid He continuous-flow cryostat operating at 4 K. The cryostat is mounted on an  $x$ - $y$ - $z$  translation stage, for tuning its position, with a base structure conceived to reduce the vibrations and the thermal drifts. The helium dewar is kept suspended by the optical table, which significantly reduces vibrations on the sample from the ground. In order to monitor the stability of the measurements, we image the sample surface with the excitation laser spot on a CCD camera as described above. We control then the stability of the laser-spot position with respect to the mesa pattern during the experiment. The sample remains stable without drift from its initial position during minutes, which is long enough for the typical data-acquisition time.

## C. Sample characterization

### 1. Polaritonic and photonic dispersion

To characterize the sample emission in the strong- and weak-coupling regimes, we perform the experiments by focusing the laser beam to a spot size of 25  $\mu\text{m}$ . The photoluminescence at low excitation power gives directly in  $k$  space the image of the energy dispersion of the polariton modes with the system in the strong coupling, which reveals the LP and UP energy bands [Fig. 2(a)]. The relaxation of polaritons results in the population being distributed in the LP and UP energy  $S$  band with the highest intensity emission from the LP band. The weak emission of UP at higher energy originating from the  $P$  bands can be perceived. Notice, this feature is better observed for UP bands because of the positive detuning of the sample. Under high excitation power when the strong coupling breaks down, we assess the energy dispersion of the photonic bands [Fig. 2(b)]. We observe the emission from the  $S$  and  $P$  photonic bands, which are formed, respectively, by evanescent coupling of  $s$  and  $p$  photon states confined in the mesas. At a higher energy, the emission from the two-dimensional photonic continuum is perceived as a faint emission around 1.492 eV: this is confirmed by the positive detuning of the two-dimensional photonic band (+8.4 meV), which is measured on the planar part of the microcavity. The origin of the two  $S$  and  $P$  photonic bands is thus well established as they lie at a lower energy.

We use a simple tight-binding approach to describe the microcavity polariton modes in a triangular lattice made out of isolated mesas. As the lattice period is larger than the mesa diameter, the coupling between next-nearest-neighbor mesas is weak. We consider only the photonic modes with the lowest energies in a single mesa: the lowest energy state (referred as the  $S$ -orbital mode) has an angular momentum equal to zero; the next excited state is doubly degenerate (referred as the two  $P$ -orbital modes) and

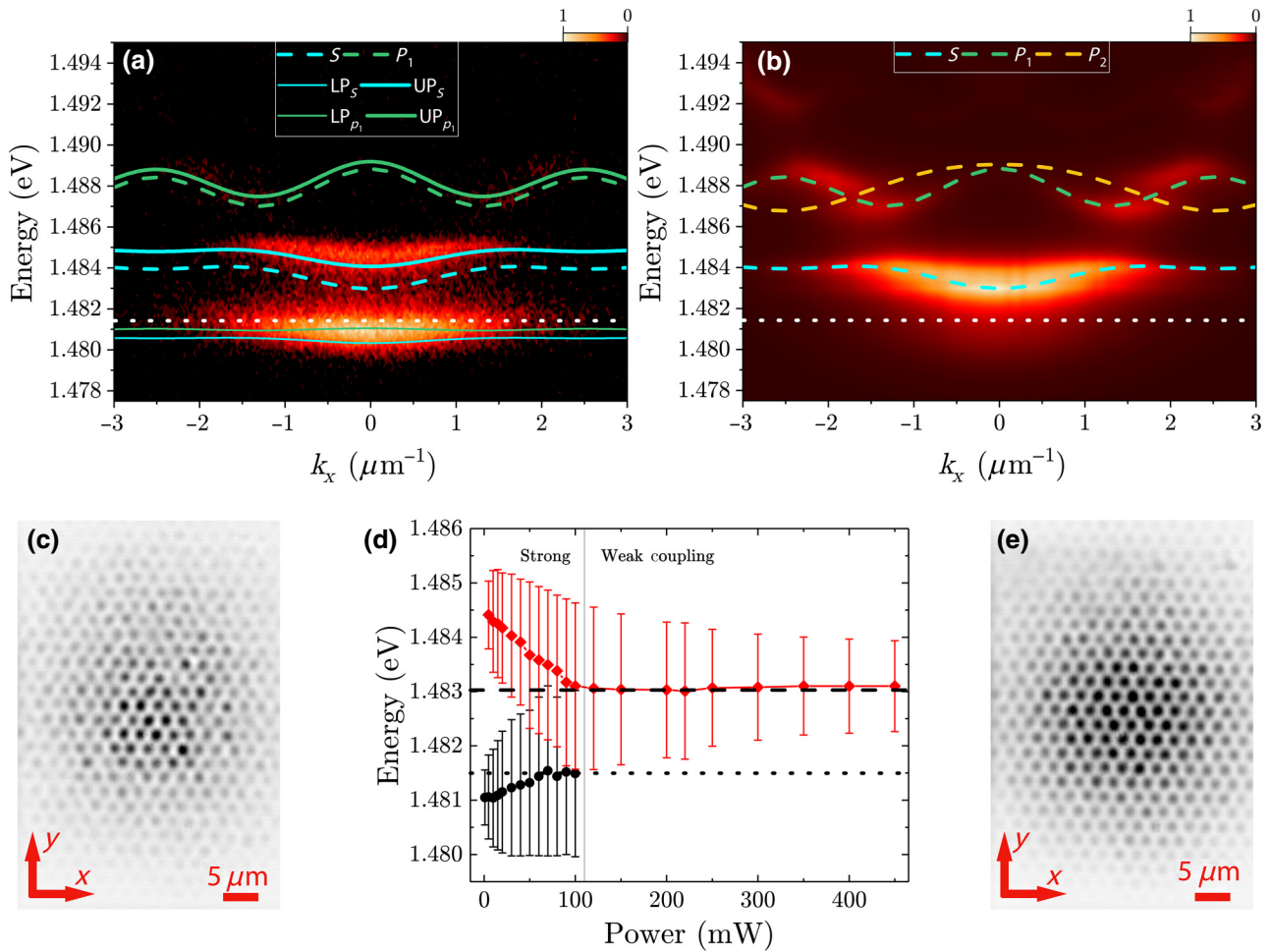


FIG. 2. Triangular photonic lattice under nonresonant laser excitation with a 25- $\mu\text{m}$  spot size. The emission spectra recorded along the  $\Gamma$ -K direction of the Brillouin zone at excitation power of 5 mW (a) and 450 mW (b), respectively, in the strong- and weak-coupling regime. The calculated LP and UP  $S$  and  $P$  dispersion bands (photonic bands) are plotted with solid lines (dashed lines). The intensity profile of the energy-integrated emission measured in the strong- (c) and the weak- (e) coupling regime. (d) Energy and linewidth of the  $S$ -band emission at  $k = 0$  as a function of pump power for the lower (black) and upper (red) polariton in the regime of strong coupling and for the photon in the weak-coupling regime. The linewidth of the modes is represented as an error bar. The dotted (dashed) line indicates the exciton ( $S$  photon mode at  $k = 0$ ) energy.

is associated to an angular momentum equal to one. The expressions for the energy dispersion of the  $S$  and  $P$  photonic bands of the triangular lattice are, respectively, given by

$$E^S = E_0^S - \gamma_0 - \gamma_S \left\{ 4 \cos \frac{a}{2} k_x \cos \frac{a}{2} \sqrt{3} k_y + 2 \cos a k_x \right\}, \quad (1)$$

$$E_{1,2}^P = \frac{(E_1 + E_2)}{2} \mp \sqrt{(E_1 - E_2)^2 + 4E_3^2}, \quad (2)$$

where

$$E_1 = E_0^P - \gamma_1 + 2\gamma_{//} \cos a k_x + (\gamma_{//} - 3\gamma_{\perp}) \cos \frac{a}{2} \sqrt{3} k_y \cos \frac{a}{2} k_x, \quad (3)$$

$$E_2 = E_0^P - \gamma_2 - 2\gamma_{\perp} \cos a k_x + (3\gamma_{//} - \gamma_{\perp}) \cos \frac{a}{2} \sqrt{3} k_y \cos \frac{a}{2} k_x, \quad (4)$$

$$E_3 = -\gamma_3 \sin \frac{a}{2} \sqrt{3} k_y \sin \frac{a}{2} k_x, \quad (5)$$

$E_0^S$ ,  $E_0^P$  are the energies of the  $S$  and  $P$  photon modes of an isolated mesa;  $\gamma_{//}$  and  $\gamma_{\perp}$  are the tunneling energies between nearest mesas associated to the  $P$  orbitals oriented either parallel or perpendicular to the link direction;  $\gamma_S$  is the tunneling energy associated to the coupling of  $S$  orbitals between nearest mesas;  $\gamma_3$  is the tunneling energy associated to the coupling between  $P_x$  and  $P_y$  orbitals centered on nearest mesas;  $\gamma_0$ ,  $\gamma_1$ ,  $\gamma_2$  are corrective energies for the photonic modes in isolated mesas. We notice that

the dispersion relations of the photonic  $P$  bands are simply given by the expressions for  $E_1$  and  $E_2$  along specific directions of the Brillouin zone, e.g.,  $\Gamma$ -K for which  $k_y$  is equal to zero or  $\Gamma$ -M for which  $k_x$  is equal to zero. The corresponding polaritonic  $S$  and  $P$  bands are obtained in the strong-coupling limit between excitons and photons assuming the same Rabi-coupling energy for the two photonic modes ( $S$  and  $P$  modes).

The calculated polaritonic and photonic  $S$  and  $P$  bands are plotted, respectively, in Figs. 2(a) and 2(b). We use the following values of the parameters for the fittings:  $\gamma_S = 0.12$  meV,  $E_0^S - \gamma_0 = 1.48370$  eV,  $E_0^P - \gamma_1 = 1.48781$  eV,  $E_0^P - \gamma_2 = 1.48803$  eV,  $\gamma_{\parallel} = 0.40$  meV,  $\gamma_{\perp} = 0.067$  meV. For these values, the polaritonic and photonic energy bands observed in the experiments are well reproduced. However, the second  $P$  band is not observed for still unclear reasons. It is worth mentioning that the tunneling energy parallel to the link direction is much larger than the one perpendicular to the link as expected from the larger overlap of the  $P$  orbitals aligned along the link joining nearest mesas with respect to the  $P$  orbitals oriented orthogonal to the link.

## 2. Polaritonic and photonic features and lattice landscape

We obtain the intensity profiles of the polaritonic and photonic lattice landscape by imaging in real space the energy integrated emission of the sample, respectively, in the strong- [Fig. 2(c)] and weak-coupling [Fig. 2(e)] regimes. In Fig 2(d), we plot the energy of the LP and UP  $S$ -band emission at  $k = 0$  as a function of pump power. We evidence with increasing pump power a blueshift of the LP,

a redshift of the UP, and a broadening of their linewidth (represented by error bars). We finally observe the shrinkage of the Rabi coupling and the emission from the photonic mode dispersion with its linewidth narrowing accordingly. These findings evidence the features characterizing the breakdown of the exciton-photon strong coupling. In nonresonant excitation, electrons and holes are generated at high energy and relax down to form excitons and polaritons. The exciton-exciton interactions induce decoherence and accordingly linewidth broadening of polaritons [36]. The exciton oscillator strength weakens when the carrier density is increased due to Coulomb screening and phase-space filling [37]. These effects reduce the coherent coupling between exciton and photon until its breakdown. We notice that the strong coupling persists in the periphery of the excitation area, where the carrier density is much weaker. Therefore, the measured linewidth of the photon dispersion appears broader than in the case of the bare photonic emission.

## III. LOCALIZED PHOTON LASING AND THE GENERATED DEFECT

To establish the localization of photon lasing emission, we perform the experiments by focusing the laser onto a spot size of  $3 \mu\text{m}$  and by centering it on top of a mesa. The integrated emission intensity as a function of laser power is displayed in Fig. 3(a). By increasing the excitation power, the system undergoes a succession of two-phase transitions; first, in breaking the strong coupling of the exciton photon, then the system evolves in the weak-coupling regime until it finally attains the laser phase transition due to the onset of the stimulated emission of photons into the

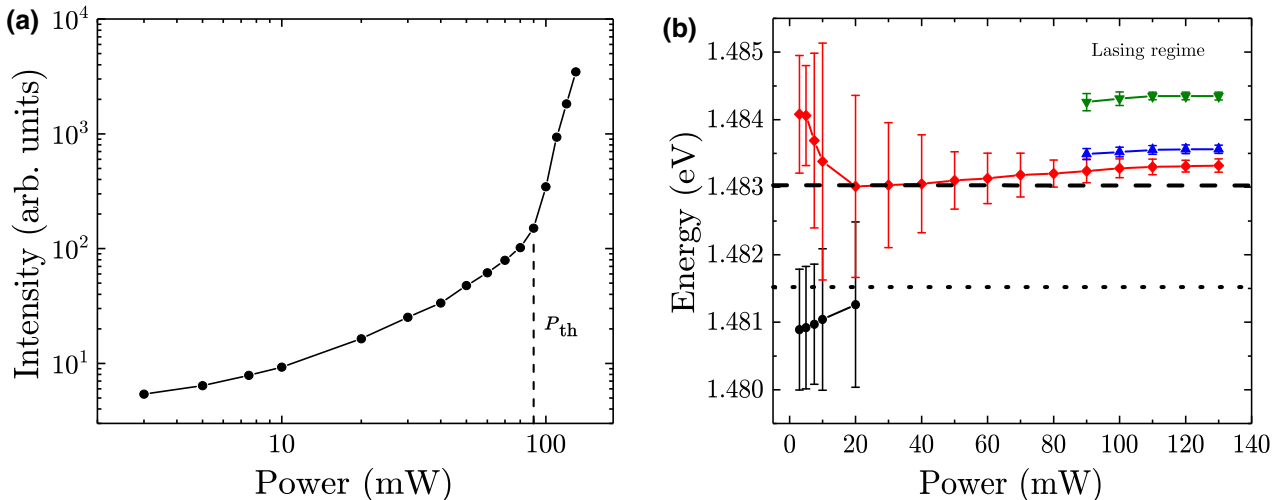


FIG. 3. Photon lasing in triangular polaritonic lattice under nonresonant excitation with a  $3\text{-}\mu\text{m}$  spot centered on top of a mesa. (a) Integrated emission intensity as a function of excitation power. The lasing phase transition is evidenced by the threshold in the power dependence ( $P_{\text{th}}$ ). (b) The emission energy at  $k = 0$  of the lower (black) and upper (red) polariton in strong coupling and of the cavity photon (red) in weak coupling; in the lasing regime, the energy of the confined lasing modes. Their linewidth is represented as error bars. The dotted (dashed) horizontal line is drawn at the exciton (photon) energy at  $k = 0$ .

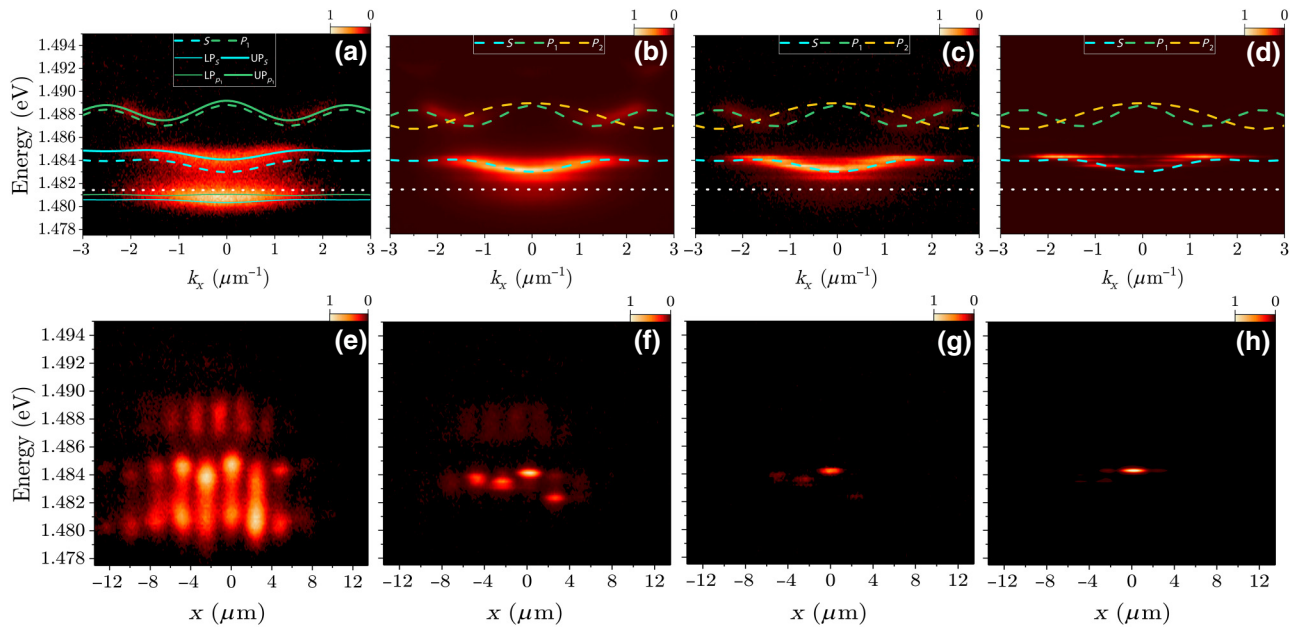


FIG. 4. Emission spectra under nonresonant excitation with a 3- $\mu\text{m}$  spot size. The energy-resolved emission measured in momentum space along the  $\Gamma$ -K direction (a)–(d) and the corresponding spectra measured in real space along the  $x$  direction (e)–(h) for four excitation powers: (a), (e)  $P = 3$  mW in strong coupling, (b), (f)  $P = 70$  mW in weak coupling, (c), (g)  $P = 90$  mW, the lasing threshold power and (d), (h)  $P = 130$  mW in the lasing regime. The calculated energy dispersion of lower and upper polaritons for the  $S$  and  $P$  bands (solid lines) and the corresponding photonic bands (dashed lines) are plotted in (a)–(d).

cavity photon mode. This is observed by the superlinear transition in the relation of the input-output light above the threshold power  $P_{\text{th}}$ . Two effects come into play with carrier density, the energy blueshift of the exciton states due to the repulsive nature of the interactions and the renormalization of the band gap in reaching the Mott transition, which corresponds to the phase transition from the exciton gas to electron-hole plasma [38]. The photon lasing takes place when the gain for the photon modes exceeds their losses.

In Fig. 3(b), we plot the energy of the emission at  $k = 0$  of the LP and UP modes in the strong-coupling case and of the cavity photon in the weak-coupling case. In the lasing regime, we plot the energy of the confined lasing modes. We show the specific features characterizing the three regimes with rising excitation power: the energy renormalization of the LP and UP modes with their linewidth broadening in the strong coupling, the linewidth narrowing of the photon-mode emission across the weak-coupling regime and three modes with a sharp linewidth characterizing a laser emission. Also, a blueshift in the laser emission is evidenced with the increasing pump power and hence the carrier density, which originates from a decrease of the refractive index in the active region.

The emission spectra showing the characteristics of the different regimes are displayed in momentum and real space for different excitation powers, respectively in Figs. 4(a)–4(d) and 4(e)–4(h). The energy dispersion of

the LP and UP bands and that of the photonic bands are plotted, respectively, in Fig. 4(a) for the strong-coupling regime and in Figs. 4(b)–4(d) for the weak-coupling regime together with the calculated polaritonic and photonic  $S$  and  $P$  bands. In real space, the emission shows an extended distribution in the strong-coupling

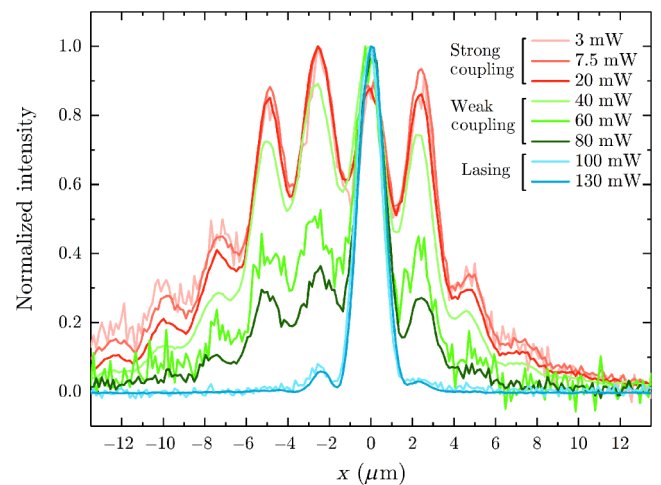


FIG. 5. Evolution of the emission spatial distribution with the excitation power under nonresonant excitation. The 3- $\mu\text{m}$  laser spot is on the mesa at  $x = 0$ .

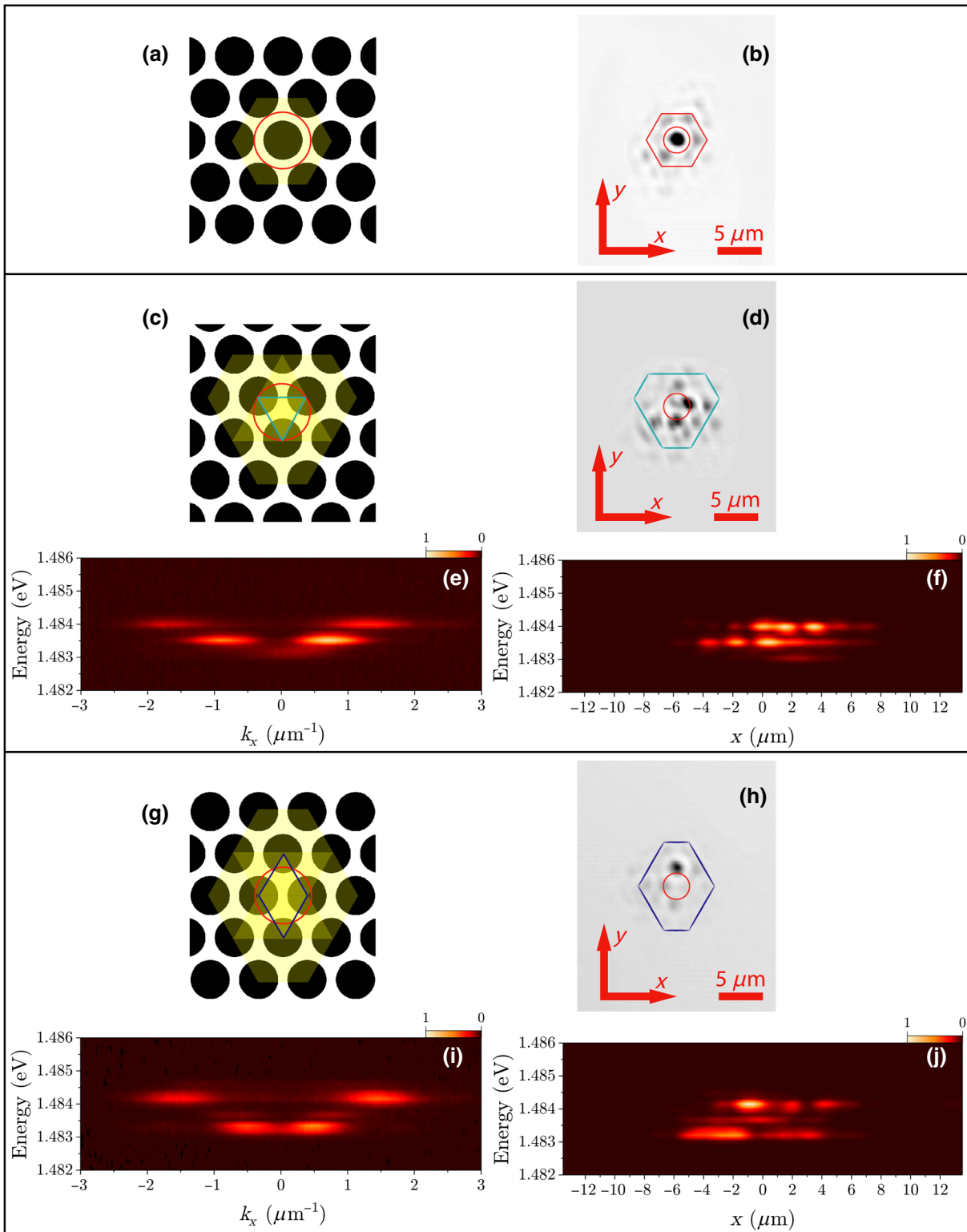


FIG. 6. Photon lasing and the induced defect with the position of the optical excitation. Representation of the triangular photonic lattice with the excited area for three different positions of the laser spot of 3- $\mu\text{m}$  size: (a) excitation on top of a mesa (red circle), (c) among three mesas (green triangle) and (g) among four mesas (blue lozenge). The hexagons drawn in yellow are composed of the excited mesas and of their six nearest neighbors; they define the region in which the defect is generated. (b), (d), (h) correspond to the energy-integrated emission in real space. The emission spectra measured in momentum space along the  $\Gamma$ -K direction (e), (i) and in real space along the  $x$  direction (f), (j) for the excitation conditions defined respectively in (c), (g). For the excitation condition defined in (a) the spectra are shown in Figs. 4(d) and 4(h). Excitation power  $P = 130$  mW. A red circle represents the position of the excitation spot. In (b), (d), and (h) the defect is highlighted by the contour zone enveloping the emitting mesas.

regime [Fig. 4(e)], which reveals the propagation of polaritons outside the excitation region. In the weak-coupling regime toward the laser phase transition, however, the spatial extension of the emission decreases [Figs. 4(f) and 4(g)] and discrete photonic modes eventually appear in  $k$  space [Fig. 4(c)]. The laser emission emerges with distinct modes, and ultimately the main emission arises at the edge of the Brillouin zone [Fig. 4(d)] like a gap soliton, the emission of which becomes mainly localized on one single mesa [Fig. 4(h)].

Near the edge of the Brillouin zone, the dispersion becomes anomalous (negative band curvature) therefore a self-defocusing nonlinearity is needed to localize a mode. The carrier density generated by the pump excitation  $I(r)$  induces a local change of the GaAs refractive index,  $n_0$ , through the Kerr effect:  $n(r) = n_0 + n_2 I(r)$ . Inside the energy gap of GaAs, the Kerr coefficient  $n_2 < 0$  is negative [39]; thus, when  $I(r)$  is increased the *local refractive index* decreases and hence an effect of self-defocusing occurs. Consequently, a localized defectlike state arises near the edge of the Brillouin zone. The local reduction of the refractive index induces the energy blueshift into the band gap [Fig. 3(d)]. This confined gap state is known in photonic crystals as a gap soliton.

We can identify two stages to the localization of the photonic modes: the first one corresponds to the creation of the photonic defect, which causes a self-trapping of the photons and the second one to the onset of lasing. In order to better evidence this sequential localization, we represent in Fig. 5 the evolution of the spatial distribution of the emission as the excitation power increases across the three regimes. In the intermediate power range corresponding to the weak-coupling regime, the spatial distribution of the emission shrinks down as the excitation power is raised. This shrinkage of the spatial distribution corresponds to the evolution of the photonic defect within the region experiencing the weak coupling. At a power of 60 mW, still well below the lasing threshold power, one observes a drastic reduction of the emission intensity from all the mesas surrounding the excitation spot, which evidences the self-trapping of photons. This is a manifestation of the local increase of the photon density, which is largest next to the excitation spot. In the last stage, as the power reaches the lasing threshold, the spatial extent of the emission collapses onto the central mesa (the mesa at position  $x = 0$ ).

The breaking of the strong-coupling regime inside a small excitation area perturbs the periodicity of the lattice and generates a defect. The arrangement and the number of mesas in this defect area define the extent of the photonic modes. The decrease of propagation losses outside this region favors the increase of the photon density by spontaneous emission due to electron-hole recombination and so optimizes the buildup of the photon-mode gain. We validate experimentally the dependence of the photon lasing

action on the induced defect by controlling the position of the optical excitation on the patterned sample.

The effect of the excitation position on the generation of the defect and the lasing emission is evidenced in Fig. 6. The number of mesas composing the defect [outlined in yellow in Figs. 6(a), 6(c) and 6(g)] is found to strongly depend on the position of the laser spot (identified as a red circle): it lies either on top of a mesa [Fig. 6(a)] or among three [Fig. 6(c)] or four [Fig. 6(g)] mesas. In Fig. 6(b), we display the spatial distribution of the total emission intensity integrated in energy when the excitation spot is on top of a mesa [corresponding to the conditions of Figs. 4(d) and 4(h)]: the predominant emission arises then from one mesa surrounded by six weakly emitting mesas. The spatial shape of the defect involves seven mesas altogether: it is the hexagon formed by the six nearest-neighbor mesas surrounding the mesa from which most of the lasing-mode emission originates. We highlight the defect extension by a hexagon that contains the mesas emitting in the weak-coupling regime. In Figs. 6(d) and 6(h) we display similarly the spatial distribution of the total emission intensity when the excitation position is displaced off a mesa and is surrounded by either three [Fig. 6(d)] or four [Fig. 6(h)] mesas. We observe distinct emission patterns spread over several mesas. We reproduce the emission zone and the arrangement of the mesas involved in the defect formation by superposing the hexagons built from the six nearest-neighbor mesas of each mesa constituting the group of three (green) and four (blue) mesas in Figs. 6(c) and 6(g). Therefore, the generated defect shapes differ from one to the others [Figs. 6(a), 6(c) and 6(g)]. We represent in Figs. 6(d) and 6(h) the contour of the defect zone with the emitting mesas inside. We plot the corresponding measured energy of the lasing emission in momentum [Figs. 6(e) and 6(i)] and real [Figs. 6(f) and 6(j)] space, for which the emission pattern of mesas in real space and their momentum distribution can be associated. We can identify mainly two lasing supermodes originating from the coupling of the mesas situated inside the defect region. From this comparison, we infer that the configuration of the defect during its generation ultimately defines the emission mode and its characteristic spatial distribution. With these results we highlight the possibility of controlling the defect geometry and ultimately the lasing mode.

#### IV. CONCLUSIONS

In conclusion, we demonstrate the realization of photon lasing integrated in a polaritonic lattice for which the lasing mode can be optically controlled. The scheme is based on the optical breaking of the translational symmetry through the local transition from the strong- to the weak-coupling regime of the exciton-photon system that is created inside a semiconductor microcavity patterned with a triangular lattice of mesas. In this way, we demonstrate

self-trapping of light and localized photon lasing. The lasing modes originate from the interplay of the photonic confinement and photon propagation, which can be controlled by the position of the excitation. These results open the way for the realization of localized mode lasers of chosen geometry, in which the shape of the generated defect determines the lasing mode. This scheme can be extended to realize chiral microlasers using optical breaking of time-reversal symmetry in a two-dimensional semiconductor honeycomb patterned microcavity [40]. One might conceive the realization of *PT* (parity and time-reversal) symmetry breaking with optical control of gain and loss [41,42]. It is also feasible to develop drop and add filters [43,44] and dynamic photon pinning [45] using optically controlled defect cavities and line-defect waveguides in two-dimensional polaritonic lattices.

- [1] J. D. Joannopoulos, R. B. Meade, and J. N. Winn, *Photonic Crystals* (Princeton University Press, Princeton, 1995).
- [2] D. N. Christodoulides, F. Lederer, and Y. Silberberg, Discretizing light behaviour in linear and nonlinear waveguide lattices, *Nature* **424**, 817 (2003).
- [3] D. N. Christodoulides and R. I. Joseph, Discrete self-focusing in nonlinear arrays of coupled waveguides, *Opt. Lett.* **13**, 794 (1988).
- [4] J. W. Fleischer, M. Segev, N. K. Efremidis, and D. N. Christodoulides, Observation of two-dimensional discrete solitons in optically induced nonlinear photonic lattices, *Nature* **422**, 147 (2003).
- [5] F. Lederer, G. I. Stegeman, D. N. Christodoulides, G. Assanto, M. Segev, and Y. Silberberg, Discrete solitons in optics, *Phys. Rep.* **463**, 1 (2008).
- [6] Z. Chen, M. Segev, and D. N. Christodoulides, Optical spatial solitons: Historical overview and recent advances, *Rep. Prog. Phys.* **75**, 086401 (2012).
- [7] S. F. Mingaleev and Y. S. Kivshar, Self-trapping and Stable Localized Modes in Nonlinear Photonic Crystals, *Phys. Rev. Lett.* **86**, 5474 (2001).
- [8] J. P. Dowling, M. Scalora, M. J. Bloemer, and C. M. Bowden, The photonic band edge laser: A new approach to gain enhancement, *J. Appl. Phys.* **75**, 1896 (1994).
- [9] K. Inoue, M. Sasada, J. Kawamata, K. Sakoda, and J. W. Haus, A two-dimensional photonic crystal laser, *Jpn. J. Appl. Phys.* **38**, L157 (1999).
- [10] M. Meier, A. Mekis, A. Dodabalapur, A. Timko, R. E. Slusher, J. D. Joannopoulos, and O. Nalamasu, Laser action from two-dimensional distributed feedback in photonic crystals, *Appl. Phys. Lett.* **74**, 7 (1999).
- [11] S. Boutami, B. Ben Bakir, P. Regreny, J. L. Leclercq, and P. Viktorovitch, Compact  $1.55\mu\text{m}$  room-temperature optically pumped VCSEL using photonic crystal mirror, *Electr. Lett.* **43**, 282 (2007).
- [12] H.-Y. Ryu, S.-H. Kwon, Y.-J. Lee, Y.-H. Lee, and J.-S. Kim, Very-low-threshold photonic band-edge lasers from free-standing triangular photonic crystal slabs, *Appl. Phys. Lett.* **80**, 3476 (2002).
- [13] E. Yablonovitz, Inhibited Spontaneous Emission in Solid-State Physics and Electronics, *Phys. Rev. Lett.* **58**, 2059 (1987).
- [14] E. M. Purcell, Spontaneous emission probabilities at radio frequencies, *Phys. Rev.* **69**, 681 (1946).
- [15] K. Srinivasan, P. Barclay, O. Painter, J. Chen, C. Cho, and C. Gmachl, Experimental demonstration of a high quality factor photonic crystal microcavity, *Appl. Phys. Lett.* **83**, 1915 (2003).
- [16] Y. Akahane, T. Asano, B.-S. Song, and S. Noda, High-Q photonic nanocavity in a two-dimensional photonic crystal, *Nature* **284**, 944 (2003).
- [17] O. Painter, R. K. Lee, A. Scherer, A. Yariv, J. D. O'Brien, P. D. Dapkus, and I. Kim, Two-dimensional photonic band-Gap defect mode laser crystals, *Science* **284**, 1819 (1999).
- [18] H.-G. Park, J.-K. Hwang, J. Huh, H.-Y. Ryu, Y.-H. Lee, and J.-S. Kim, Nondegenerate monopole-mode two-dimensional photonic band gap laser, *App. Phys. Lett.* **79**, 3032 (2001).
- [19] L. J. Martinez, B. Alén, I. Prieto, D. Fuster, L. Gonzalez, Y. Gonzalez, M. L. Dotor, and P. A. Postigo, Room temperature continuous wave operation in a photonic crystal microcavity laser with a single layer of InAs/InP self-assembled quantum wires, *Opt. Express* **17**, 14993 (2009).
- [20] C. Weisbuch, M. Nishioka, A. Ishikawa, and Y. Arakawa, Observation of the Coupled Exciton-Photon Mode Splitting in a Semiconductor Quantum Microcavity, *Phys. Rev. Lett.* **69**, 3314 (1992).
- [21] I. Carusotto and C. Ciuti, Quantum fluids of light, *Rev. Mod. Phys.* **85**, 299 (2013).
- [22] A. Amo and J. Bloch, C. R. exciton-polaritons in lattices: A non-linear photonic simulator, *Physique* **17**, 934 (2016).
- [23] T. Jacqmin, I. Carusotto, I. Sagnes, M. Abbarchi, D. D. Solnyshkov, G. Malpuech, E. Galopin, A. Lemaître, J. Bloch, and A. Amo, Direct Observation of Dirac Cones and a Flat-band in a Honeycomb Lattice for Polaritons, *Phys. Rev. Lett.* **112**, 116402 (2014).
- [24] D. Tanese, H. Flayac, D. Solnyshkov, A. Amo, A. Lemaître, E. Galopin, R. Braive, P. Senellart, I. Sagnes, G. Malpuech, and J. Bloch, Polariton condensation in solitonic gap states in a one-dimensional periodic potential, *Nat. Commun.* **4**, 1749 (2013).
- [25] M. Milicevic, O. Bleu, D. D. Solnyshkov, I. Sagnes, A. Lemaître, L. Le Gratiet, A. Harouri, J. Bloch, G. Malpuech, and A. Amo, Lasing in optically induced gap states in photonic graphene, *SciPost Phys.* **5**, 064 (2018).
- [26] K. Winkler, J. Fischer, A. Schade, M. Amthor, R. Dall, J. Geßler, M. Emmerling, E. A. Ostrovskaya, M. Kamp, C. Schneider, and S. Höfling, A polariton condensate in a photonic crystal potential landscape, *New J. Phys.* **17**, 023001 (2015).
- [27] K. Winkler, O. A. Egorov, I. G. Savenko, X. Ma, E. Estrecho, T. Gao, S. Müller, M. Kamp, T. C. H. Liew, E. A. Ostrovskaya, S. Höfling, and C. Schneider, Collective state transitions of exciton-polaritons loaded into a periodic potential, *Phys. Rev. B* **93**, 121303 (2016).
- [28] H. Pier, E. Kapon, and M. Moser, Strain effects and phase transitions in photonic resonator crystals, *Nature* **407**, 880 (2000).

- [29] L. D. A. Lundeberg, D. L. Boiko, and E. Kapon, Coupled islands of photonic crystal heterostructures implemented with vertical-cavity surface-emitting lasers, *App. Phys. Lett.* **87**, 241120 (2005).
- [30] L. Mutter, V. Iakovlev, A. Caliman, A. Mereuta, A. Sirbu, and E. Kapon, 1.3 $\mu$ m-wavelength phase-locked VCSEL arrays incorporating patterned tunnel junction, *Opt. Express* **17**, 8558 (2009).
- [31] D.-S. Song, S.-H. Kim, H.-G. Park, C.-K. Kim, and Y.-H. Lee, Single-fundamental-mode photonic-crystal vertical-cavity surface-emitting lasers, *App. Phys. Lett.* **80**, 3901 (2002).
- [32] J. J. Raftery, A. J. Danner, J. C. Lee, and K. D. Choquette, Coherent coupling of two-dimensional arrays of defect cavities in photonic crystal vertical cavity surface-emitting lasers, *Appl. Phys. Lett.* **86**, 201104 (2005).
- [33] B. G. Griffin, A. Arbabi, M. P. Tan, A. M. Kasten, K. D. Choquette, and L. L. Goddard, Demonstration of enhanced side-mode suppression in metal-filled photonic crystal vertical cavity lasers, *Opt. Lett.* **38**, 1936 (2013).
- [34] P. Nyakas, Honeycomb photonic crystal vertical-cavity surface-emitting lasers: Coupled cavities enhancing the single-mode range, *J. Opt. Soc. Am. B* **30**, 3284 (2013).
- [35] R. Idrissi Kaitouni, O. El Daif, A. Baas, M. Richard, T. Paraiso, P. Lugan, T. Guillet, F. Morier-Genoud, J. D. Ganière, J. L. Staehli, V. Savona, and B. Deveaud, Engineering the spatial confinement of exciton polaritons in semiconductors, *Phys. Rev. B* **74**, 1553311 (2006).
- [36] N. Takemura, M. D. Anderson, S. Trebaol, S. Biswas, D. Y. Oberli, M. T. Portella-Oberli, and B. Deveaud, Dephasing effects on coherent exciton-polaritons and the breakdown of the strong coupling regime, *Phys. Rev. B* **92**, 235305-1-7 (2015).
- [37] S. Schmitt-Rink, D. S. Chemla, and D. A. Miller, Theory of transient excitonic optical nonlinearities in semiconductor quantum-well structures, *Phys. Rev. B* **32**, 6601 (1985).
- [38] L. Kappei, J. Szczytko, F. Morier-Genoud, and B. Deveaud, Direct Observation of the Mott Transition in an Optically Excited Semiconductor Quantum Well, *Phys. Rev. Lett.* **94**, 147403 (2005).
- [39] J. S. Aitchison, D. C. Hutchings, J. U. Kang, G. I. Stegeman, and A. Villeneuve, The nonlinear optical properties of AlGaAs at the half band gap, *IEEE J. Quant. Electr.* **33**, 341 (1997).
- [40] N. C. Zambon, P. St-Jean, M. Milićević, A. Lemaître, A. Harouri, L. Le Gratiet, O. Bleu, D. D. Solnyshkov, G. Malpuech, I. Sagnes, S. Ravets, A. Amo, and J. Bloch, Optically controlling the emission chirality of microlasers, *Nat. Photonics* **13**, 283 (2019).
- [41] C. E. Rütter, K. G. Makris, R. El-Ganainy, D. N. Christodoulides, M. Segev, and D. Kip, Observation of parity-time symmetry in optics, *Nat. Phys.* **6**, 192 (2010).
- [42] V. V. Konotop, J. Yang, and D. A. Zezyulin, Nonlinear waves in PT-symmetric systems, *Rev. Mod. Phys.* **88**, 35002 (2016).
- [43] S. Noda, A. Chutinan and M. Imada, Song and S. Noda, Trapping and emission of photons by a single defect in a photonic bandgap structure, *Nature* **407**, 608 (2000).
- [44] Y. Akahane, T. Asano, B.-S. Song, and S. Noda, Investigation of high-Q channel drop filters using donor-type defects in two-dimensional photonic crystal slabs, *Appl. Phys. Lett.* **83**, 1512 (2003).
- [45] M. Notomi and H. Taniyama, On-demand ultrahigh-Q cavity formation and photon pinning via dynamic waveguide tuning, *Opt. Express* **16**, 18657 (2008).